J|A|C|S ARTICLES

Published on Web 03/10/2009

Insights into the Kinetics of Semiconductor Nanocrystal Nucleation and Growth

Jane Y. Rempel,[†] Moungi G. Bawendi,*[,‡] and Klavs F. Jensen*[,†]

Department of Chemical Engineering and Department of Chemistry, Massachusetts Institute of Technology, Cambridge, Massachusetts 02139

Received November 23, 2008; E-mail: kfjensen@mit.edu; mgb@mit.edu

Abstract: A model is presented for the colloidal synthesis of semiconductor nanocrystals capturing the reactions underlying nucleation and growth processes. The model combines an activation mechanism for precursor conversion to monomers, discrete rate equations for formation of small-sized clusters, and continuous Fokker−Planck equation for growth of large-sized clusters. The model allows us to track the temporal evolution of the entire cluster size distribution and compute several experimental observables including mean size and size distribution. The model predicts five distinct regions: generation of monomers, small cluster formation, size distribution focusing due to precursor depletion, pseudo steady state region, and size distribution broadening, with the latter three explicitly reproducing available experimental data at larger cluster sizes. Furthermore, we identify two nondimensional parameter combinations and discuss how these can be used to guide experiments to yield a more rational approach to synthesis modification. Contrary to the common hypothesis that diffusion is essential for size distribution focusing, the model shows that focusing can be achieved under pure reaction control. In addition, the model yields new insights into the synthesis of small nanocrystals with narrow size distributions either by modulation of temperature over the duration of nanocrystal synthesis or by introduction of small quantities of additives that enhance the rate of precursor conversion to monomers. We show that for a given set of reaction parameters, there is an optimum in the duration of high temperature and additive concentration minimizing polydispersity.

Introduction

Due to the their size tunable optical properties, colloidal semiconductor nanocrystals have attracted significant attention for use in applications ranging from electroluminescent devices[1−5] to fluorescent labels for biological imaging.[6,7] In most of these applications it is essential to use nanocrystal samples that are monodisperse and highly crystalline. Much work has been devoted to developing adaptable chemistries for preparation of high quality II−VI[8−10] and III−V[11,12] compound semiconductor nanocrystals. However, despite a tremendous experimental effort in chemistry development, the underlying mechanistic processes leading to nanocrystal formation are still poorly understood. And as a result, process development has required a laborious trial-and-error approach to finding optimal set of reactants and reaction conditions to yield the desired size nanocrystals with minimal polydispersity. To reduce the amount of the demanding laboratory trials, there is a general need to develop theoretical models that can yield insights into the underlying nanocrystal formation processes and provide guidelines for the rational synthesis manipulation. There are several characteristics that an ideal model must have. First, the model must accurately capture the kinetics of nucleation and the evolution of the nanocrystal size distribution, with a single a priori assumption that only precursors are present initially. Second, the model must contain the appropriate level of detail to accurately describe experimental observations over the entire time domain of the synthetic process, including size distribution focusing and defocusing at short and long times, respectively. And last, the model must be computationally fast to allow one to scan over a broad range of experimentally relevant conditions, and also sufficiently simple to yield a set of guiding principles for rational synthesis manipulation. Availability of such a model can not only accelerate the optimization of the existing synthetic routes but also provide the fundamental understanding that is essential for the development of new material chemistries.

[†] Department of Chemical Engineering.
[‡] Department of Chemistry.

(1) Colvin, V. L.; Schlamp, M. C.; Alivisatos, A. P. *Nature* **1994**, *370* (6488), 354–357.
(2) Dabbousi, B. O.; Bawendi, M. G.; Onitsuka, O.; Rubner, M. F. *Appl. Phys. Lett.* **1995**, *66* (11), 1316–1318.
(3) Coe, S.; Woo, W. K.; Bawendi, M. G.; Bulovic, V. *Nature* **2002**, *420*, 800–803.
(4) Tessler, N.; Medvedev, V.; Kazes, M.; Kan, S.; Banin, U. *Science* **2002**, *295* (5559), 1506–1508.
(5) Caruge, J. M.; Halpert, J. E.; Wood, V.; Bulovic, V.; Bawendi, M. G. *Nat. Photonics* **2008**, *2*, 247–250.
(6) Medintz, I. L.; Uyeda, H. T.; Goldman, E. R.; Mattoussi, H. *Nat. Mater.* **2005**, *4* (6), 435–446.
(7) Michalet, X.; Pinaud, F. F.; Bentolila, L. A.; Tsay, J. M.; Doose, S.; Li, J. J.; Sundaresan, G.; Wu, A. M.; Gambhir, S. S.; Weiss, S. *Science* **2005**, *307* (5709), 538–544.
(8) Murray, C. B.; Norris, D. J.; Bawendi, M. G. *J. Am. Chem. Soc.* **1993**, *115*, 8706–8715.
(9) Li, L. S.; Pradhan, N.; Wang, Y.; Peng, X. *Nano Lett.* **2004**, *4* (11), 2261–2264.
(10) Hines, M. A.; Guyot-Sionnest, P. *J Phys. Chem. B* **1998**, *102* (19), 3655–3657.
(11) Guzelian, A. A.; Banin, U.; Kadavanich, A. V.; Peng, X.; Alivisatos, A. P. *Appl. Phys. Lett.* **1996**, *69* (10), 1432–1434.
(12) Peng, X.; Wickham, J.; Alivisatos, A. P. *J. Am. Chem. Soc.* **1998**, *120*, 5343–5344.

Table 1. Different Types of Models of Nucleation and Growth of Semiconductor Nanocrystals

model type	key findings	limitations
Classical nucleation theory (CNT)	Nucleation flux based on surface energy of particles and monomer supersaturation	No information about the size and the size distribution
Growth law for a single particle	Evolution of the particle radius with time	Ignores monomer depletion, lack of mass conservation. No information about particle concentration or size distribution
Combination of CNT and growth law	Coupling of the nucleation flux with growth	Requires seeding of the initial distribution
Rate equation based models	Evolution of the entire size distribution with time	Computationally intensive

There are several classes of models that have been used in the past to describe the nanocrystal formation process: classical nucleation theory (CNT), single particle growth laws, a combination of the CNT and a growth law, and rate equation based models. The information gained from the different classes of models and their associated shortcomings are summarized in Table 1. CNT is frequently used to predict the rate of generation of critical sized clusters based on solution supersaturation and nanocrystal surface tension.[13] A major disadvantage of this approach is that characteristic critical nuclei sizes considered by CNT are on the order of a few nanometers, which are approximately equal to the final nanocrystal sizes, making CNT unsuitable to describe nucleation at the nanoscale. On a more practical note, CNT lacks information about the resulting size distribution of the nuclei and the subsequent growth process, both of which are essential aspects of the nanocrystalline formation process. To describe the growth of nanocrystals, single spherical particle first order reaction diffusion model has been utilized.[14,15] However, diffusion limited growth model has not been successful in reproducing experimental results over a broad range of reaction times[16] due to some fundamental limitations. First, a major drawback of the model is that it lacks mass conservation, since it does not take into account the depletion of monomers during the growth process. Second, this type of a model does not provide any information about the particle size distribution. To overcome these limitations, work has been done on simulating the growth of ensembles of nanocrystals using reaction-diffusion growth law equations individually or in combination with CNT.[15] Even though simulating an ensemble of nanocrystals yields information on the evolution of the size distribution, this type of an approach requires an a priori assumption about the initial shape of the distribution, which determines the resulting model predictions. Notably, the growth law models for a single particle or an ensemble of particles have been used to ubiquitously support the hypothesis that size distribution focusing, an experimentally observed phenomenon, is due to diffusion limited growth.[12,15,17,18] However, our estimates of the diffusion limited growth rate are several orders of magnitude higher than those observed experimentally, thus putting into question the validity of this hypothesis. As a result, one of the main objectives of the present work is to test whether size distribution focusing can be achieved under pure reaction control.

Rate equation based models are formulated by developing expressions to describe the rates of change of different sized clusters, and then solving the expressions to evolve the complete size distribution as a function of time. Since these models explicitly consider different sized clusters, they have a potential to overcome the lack of size distribution information inherent in the CNT and growth law based approaches. Mantzaris has combined a population balance approach with a reaction diffusion model for a single particle to track the evolution of the size distribution with variations in supersaturation.[19] However, seeding of the initial distribution was applied thus capturing only the growth process and lacking any insight into the early stage nucleation events. Robb et al. have combined burst nucleation, characterized by thermal equilibration of small sized clusters, with a continuous master equation for clusters of sizes greater than the critical size assuming diffusion limited growth.[20] In this case, the distribution was seeded either with a thermal distribution for subcritical clusters or in combination with a normal distribution for supercritical clusters. Therefore, most of the models thus far have required an a priori assumption for the initial size distribution, a limitation that our work aims to overcome.

The goal of this work is to develop a simple and general model to describe kinetics of the colloidal nanocrystal formation that captures the underlying chemistry, matches the experimental observations over the entire time domain of nucleation and growth, and yields a deeper fundamental understanding of the synthetic process. The general framework of the model consists of rate equations for precursor conversion to monomers and monomer attachment and detachment to clusters leading to growth and dissolution. Cluster formation is modeled by a combination of a set of discrete rate equations and a continuous Fokker−Planck equation for small and large clusters, respectively. This formalism allows us to accurately track the entire size distribution as a function of time with minimal computational intensity. The model is further simplified by nondimensionalization reducing the number of variables and constants to only two grouped parameters. The model predictions are compared to the experimental observations to show that the model predicts both size distribution focusing and defocusing on different time scales. Moreover, the model shows that focusing is obtained under pure reaction control in the absence of diffusion limitation. Taking advantage of the simplicity of the reduced model with only two key parameters, we gain insight into the nanocrystal formation process, which can be applied to rationally guide experimental process development. Finally, using the general framework of the model, we test several hypotheses for how synthesis can be modified to minimize size polydispersity in generation of small sized nanocrystals.

(13) Mullin, J. W. *Crystallization*, 4th ed.; Butterworth Heinemann: Boston, 2001.
(14) Bullen, C. R.; Mulvaney, P. *Nano Lett.* **2004**, *4* (12), 2303–2307.
(15) Talapin, D. V.; Rogach, A. L.; Haase, M.; Weller, H. *J. Phys. Chem.* **2001**, *105*, 12278–12285.
(16) Varghese, N.; Biswas, K.; Rao, C. N. R. *Chem.−Asian J.* **2008**, *3*, 1435–1442.
(17) Dushkin, C. D.; Saita, S.; Yoshie, K.; Yamaguchi, Y. *Adv. Colloid Interface Sci.* **2000**, *88*, 37–78.
(18) Peng, Z. A.; Peng, X. *J. Am. Chem. Soc.* **2002**, *124*, 3343–3353.
(19) Mantzaris, N. V. *Chem. Eng. Sci.* **2005**, *60*, 4749–4770.
(20) Robb, D. T.; Privman, V. *Langmuir* **2008**, *24* (1), 26–35.

Model Description

One strategy that has proved successful in the formation of monodisperse nanocrystal samples of high crystallinity is the liquid phase colloidal synthesis. In a typical preparation route, precursors are injected into a high temperature solvent and ligand mixture leading to fast nucleation followed by a reduced temperature slow growth. Initially dimethylcadmium was used as a group II precursor and tri-*n*-octylphosphine selenide or telluride or bis(trimethylsilyl)sulfide were used as group VI precursors.[8] The solvent mixture consisted of coordinating ligands including tri-*n*-octylphospine (TOP), tri-*n*-octylphosphine oxide (TOPO), and phosphonic acid impurities and degradation products that served to both block reaction sites on the nanocrystals and to sterically passivate nanocrystals preventing aggregation. It is worth noting that organometallic compounds that are pyrophoric, toxic, and difficult to work with have been slowly replaced with less hazardous and more stable metal salt precursors[21,22] and the number of different types of ligands used has been expanded significantly.

To model the synthesis, we consider a well-mixed system of precursors, P, that can react to form monomeric species, C_1. With only a few studies that have been aimed at understanding the chemical mechanism of nanocrystal formation,[23,24] the nature of the monomeric species that participate in growth is still largely unknown. Thus, for simplicity, we assume that there is only one rate-limiting reaction step and that the reaction is irreversible and first order in the precursor concentration, as evident from a single exponential decay in precursor concentration:[23]

$$P \xrightarrow{k_f} C_1 \tag{1}$$

where k_f is the rate constant for monomer formation. Note that binary semiconductor nanocrystals are generally prepared from two precursors; however, variation in precursor reactivity justifies the use of eq 1, with the monomeric unit containing atoms of both types. Once the monomeric species are formed, they can combine to form dimers, dimers can further react with monomers to form trimers, and so on. In a typical preparation of nanocrystals, bulky ligands are used to sterically stabilize the growing clusters and since larger clusters have more binding sites for ligand attachment, aggregation of nonmonomeric sized clusters is highly unlikely. Thus, given the slower rates of aggregation and significantly lower concentrations of nonmonomeric clusters during nucleation, we assume that only monomers significantly contribute to nanocrystal formation. The growth and dissociation reactions via monomer attachment and detachment for an n-sized cluster, C_n, can be described by:

$$C_n + C_1 \underset{D_{n+1}}{\overset{G_n}{\rightleftharpoons}} C_{n+1} \tag{2}$$

where G_n and D_n are the time dependent growth and dissociation transition frequencies of monomer attachment and detachment, respectively.

Growth and Dissociation Rates. On the basis of eq 2, we can formulate kinetic expressions for evolution of the cluster concentrations. To do so requires us to develop expressions for the attachment and detachment frequencies. First, we postulate that under reaction control, the growth rate would be proportional to the number of available sites on the cluster surface and the monomer concentration. Since ligands can bind to the cluster surface and block potential sites for monomer attachment, the strength of binding and ligand concentration would determine the number of available surface sites. Second, we postulate that the cluster dissociation rate is proportional to the number of sites occupied by ligands, since ligands stabilize the monomeric units thus enhancing dissociation. Since typical concentrations of ligands are significantly higher than those of monomers leading to fast binding and ligands bind relatively weakly to clusters leading to fast dissociation, we assume that on the time scale of nanocrystal formation, free ligands are at equilibrium with those bound to the clusters. This allows us to determine the number of available or occupied sites for the calculation of monomer attachment and detachment frequencies:

$$G_n \propto N_{\text{sites},n} \frac{1}{1 + K_{\text{eq}}L} C_1 \tag{3}$$

$$D_n \propto N_{\text{sites},n} \frac{K_{\text{eq}}L}{1 + K_{\text{eq}}L} \tag{4}$$

where $N_{\text{sites},n}$ is the total number of cluster binding sites, K_{eq} is the equilibrium constant for ligand binding to clusters, and L and C_1 are the ligand and monomer concentrations, respectively. The number of surface sites is proportional to the exposed surface area; thus, assuming that the nanocrystals are approximately spherical leads to:

$$N_{\text{sites},n} = \left[\frac{\sigma}{\rho^{2/3}}(36\pi)^{1/3}\right] n^{2/3} \tag{5}$$

where σ is the number of sites per unit area and ρ is the material number density. Furthermore, the typical concentration of ligands is several orders of magnitude higher than that of nanocrystals, and as a result, the total free ligand concentration remains approximately constant throughout the reaction. These two assumptions significantly simplify the expressions in eqs 3 and 4 to:

$$G_n = k_a n^{2/3} C_1 \tag{6}$$

$$D_n = k_d n^{2/3} \tag{7}$$

where k_a and k_d are the effective rate constants, which include the intrinsic rate of monomer addition and dissociation plus a group of invariable terms: $[(\sigma)/(\rho^{2/3})(36\pi)^{1/3}]/(1 + K_{\text{eq}}L)$ and $[(\sigma)/(\rho^{2/3})(36\pi)^{1/3}](K_{\text{eq}}L)/(1 + K_{\text{eq}}L)$, respectively.

Governing Equations. On the basis of the growth and dissociation frequency definitions, we obtain the rates of change for the precursors, monomers, and a set of N discrete rate equations for clusters:

$$\frac{dP}{dt} = -k_f P \tag{8}$$

(21) Peng, Z. A.; Peng, X. G. *J. Am. Chem. Soc.* **2001**, *123*, 183–184.
(22) Qu, L.; Peng, Z. A.; Peng, X. *Nano Lett.* **2001**, *1* (6), 333–337.
(23) Liu, H.; Owen, J. S.; Alivisatos, A. P. *J. Am. Chem. Soc.* **2007**, *129* (2), 305–312.
(24) Steckel, J. S.; Yen, B. K. H.; Oertel, D. C. *J. Am. Chem. Soc.* **2006**, *128*, 13032–13033.

Table 2. Summary of the Scaled Variables and Model Parameters

Variables	$c_n = (C_n)/(P_0)$	Scaled cluster concentration
	$p = (P)/(P_0)$	Scaled precursor concentration
	$\tau = k_f t$	Scaled time
Primary Parameters	$\alpha = (k_a P_0)/(k_f)$	Scaled growth rate parameter
	$\beta = (k_d)/(k_f)$	Scaled dissociation rate parameter
Diffusion Control	$\alpha_D = (k_{a,D} P_0)/(k_f)$	Scaled growth rate parameter under diffusion limitation
Temperature Modulation	$\varepsilon_\infty = (E)/(k_B T_\infty)$	Scaled activation energy
	τ_T	Scaled temperature decay time parameter
	$(T_\infty)/(T_0)$	Ratio of final to initial temperature
Additives	$\delta = (k_{f,a} P_0)/(k_f)$	Scaled enhancement in precursor conversion rate due to additives
	$a = (A_0)/(P_0)$	Scaled initial additive concentration

$$\frac{dC_1}{dt} = k_f P - k_a C_1^2 - k_a \sum_{n=1}^{N-1} (n)^{2/3} C_n C_1 + k_d (2)^{2/3} C_2 + k_d \sum_{n=2}^{N} (n)^{2/3} C_n \quad (9)$$

$$\frac{dC_n}{dt} = k_a (n-1)^{2/3} C_{n-1} C_1 - k_d (n)^{2/3} C_n - k_a (n)^{2/3} C_n C_1 + k_d (n+1)^{2/3} C_{n+1} \quad (10)$$

where N is the maximum considered cluster size.

Non-Dimensionalization. The rate expressions, eqs 8−10, contain two dimensions for variables: concentration and time, and three rate constants: k_a, k_d, and k_f. To gain further insight into the model predictions, we introduce nondimensional concentration and time:

$$c_n = \frac{C_n}{P_0}; p = \frac{P}{P_0} \quad (11)$$

$$\tau = k_f t \quad (12)$$

where concentration is scaled by the initial precursor concentration, P_0, and time is scaled by the rate of monomer generation from precursors. Substituting these definitions into eqs 8−10 leads to:

$$\frac{dp}{d\tau} = -p \quad (13)$$

$$\frac{dc_1}{d\tau} = p - \alpha c_1^2 - \alpha \sum_{n=1}^{N-1} (n)^{2/3} c_n c_1 + \beta (2)^{2/3} c_2 + \beta \sum_{n=2}^{N} (n)^{2/3} c_n \quad (14)$$

$$\frac{dc_n}{d\tau} = \alpha (n-1)^{2/3} c_{n-1} c_1 - \beta (n)^{2/3} c_n - \alpha (n)^{2/3} c_n c_1 + \beta (n+1)^{2/3} c_{n+1} \quad (15)$$

where parameters α and β (Table 2) are defined as:

$$\alpha = \frac{k_a P_0}{k_f} \quad (16)$$

$$\beta = \frac{k_d}{k_f} \quad (17)$$

The scaled growth and dissociation frequencies become:

$$g_n = \alpha n^{2/3} c_1 \quad (18)$$

$$d_n = \beta n^{2/3} \quad (19)$$

Diffusion Control. The derivation above was presented for the case of the reaction controlled growth. However, the model can be easily adapted to incorporate a diffusion limitation. In such a case the rate of growth would be proportional to the radius of the nanocrystal as opposed to the available surface area. Thus, the scaled diffusion limited growth rate would be given by:

$$g_{n,D} = \alpha_D n^{1/3} c_1 \quad (20)$$

where the scaled parameter for addition via diffusion and the effective addition rate are defined as (Table 2):

$$\alpha_D = \frac{k_{a,D} P_0}{k_f} \quad (21)$$

$$k_{a,D} = 4\pi N_A D_{C_1} \left(\frac{3}{4\pi\rho}\right)^{1/3} \quad (22)$$

where D_{C_1} is the monomer diffusivity. Furthermore, assuming that the concentration of the monomer at the growth interface is at pseudo steady state and equating the reaction and diffusion fluxes, the effective growth rate in the special case of slow diffusion becomes:

$$g_n = \frac{\alpha_D n^{1/3} c_1 + \beta n^{2/3}}{1 + \frac{\alpha_D}{\alpha} n^{-1/3}} \quad (23)$$

Temperature Modulation. As described above, in most recent routes for batch synthesis of nanocrystals, injection of the precursors is performed into a solvent maintained at an elevated temperature relative to the ultimate growth temperature.[8] This hot injection technique can be modeled by an exponential decrease in temperature from T_0 to T_∞:

$$T = T_\infty + (T_0 - T_\infty)\exp[-\tau/\tau_T] \quad (24)$$

where τ_T is the nondimensional time constant. Note that for a well mixed fluid of initial temperature of T_0 in a vessel with surface temperature of T_∞, the nondimensional time constant can be interpreted as: $\tau_T = k_f(\rho_f C_p)/(h)(V/A)_v$, where ρ_f is the fluid density, C_p is the heat capacity, h is the heat transfer coefficient, $((V)/(A))_v$ is the volume to area ratio of the vessel.

Furthermore, we postulate that temperature primarily affects the rate limiting step of the precursor conversion to monomer. Thus, given the activation energy for the reaction, the rate of precursor consumption becomes:

$$\frac{dp}{d\tau} = -p\left[e^{\varepsilon_\infty\left(1-\frac{T_\infty}{T}\right)}\right] \quad (25)$$

This modification is also incorporated into eq 14. Description of this process requires the introduction of three new nondimensional parameters: scaled activation energy, ratio of final and initial temperature, and the temperature decay time constant (Table 2):

$$\varepsilon_\infty = \frac{E}{k_B T_\infty}; \frac{T_\infty}{T_0}; \tau_T \quad (26)$$

Additives. Additives can also play a large role in the chemistry of monomer formation either by enhancing or inhibiting the rate of precursor conversion to monomers. For example, introduction of stronger reducing agents in the form of dialkyl phosphines in place of trialkyl phosphines has been shown to significantly enhance the rate of PbSe nanocrystal formation.[24] To incorporate the effect of rate enhancing additives (A), we consider two competing reactions for monomer formation:

$$P \xrightarrow{k_f} C_1 \quad (27)$$

$$P + A \xrightarrow{k_{f,a}} C_1$$

where $k_{f,a}$ is the rate of precursor conversion to monomer in the presence of an additive. Assuming that the precursor concentration remains approximately constant and that $k_{f,a}P_0 \gg k_f$, the effective nondimensional rate for precursor conversion to monomer becomes:

$$\frac{dp}{d\tau} = -p\left[1 + \left(\frac{k_{f,a}P_0}{k_f}\right)\left(\frac{A_0}{P_0}\right)e^{-\left(\frac{k_{f,a}P_0}{k_f}\right)\tau}\right] = -p[1 + (\delta)(a)e^{-\delta\tau}] \quad (28)$$

Two new nondimensional parameters become important—the enhancement in the rate due to additives and the relative additive content (Table 2):

$$\delta = \frac{k_{f,a}P_0}{k_f} \quad (29)$$

$$a = \frac{A_0}{P_0} \quad (30)$$

Numerical Considerations. The discrete rate equations (eqs 13−15) can be integrated numerically. However, since the largest cluster size can be on the order of 10^5 monomeric units, the problem can be significantly simplified by approximating the discrete rate equations by a continuous Fokker−Planck partial differential equation (FPE). To obtain the continuous FPE approximation to eq 15, we performed a Taylor series expansion to the second order in the n-space on the $g_{n-1}c_{n-1}$ and $d_{n+1}c_{n+1}$ terms yielding:[25]

$$\frac{\partial f}{\partial \tau} = \frac{\partial}{\partial n}\left(\left[d - g + \frac{1}{2}\frac{\partial}{\partial n}(g + d)\right]f + \left[\frac{1}{2}(g + d)\right]\frac{\partial f}{\partial n}\right) \quad (31)$$

where f is the distribution as a function of the continuous size domain, n, and scaled time, τ. Note that the Taylor series expansion is only accurate for large sizes ($n \gg 1$); as a result, we employed discrete rate equations for small clusters ($n < n_{match}$), the FPE for large clusters, and a modified conservation equation for the monomers:

$$\frac{dc_1}{d\tau} = p - \sum_{n=1}^{n_{match}} n\frac{dc_n}{d\tau} - \int_{n_{match}}^{n_{max}} n\frac{\partial f}{\partial \tau}dn \quad (32)$$

where n_{match} is the matching point and n_{max} is the maximum considered cluster size. Note that n_{max} must be chosen sufficiently large to diminish its effect on the numerical solution. Two new boundary conditions were introduced with the discrete and continuous concentrations and fluxes matched at n_{match} and the no-flux boundary condition applied at n_{max}. The Chang-Cooper (CC70) weighted finite difference scheme[26−28] was applied to discretize the n-dependent part of the FPE, as described in detail in the Supporting Information. The weighting coefficients in the CC70 method were determined by explicitly equating the exact and approximate fluxes leading to a nonnegative and particle conserving solution. A power law expression was applied for the finite difference mesh spacing of the FPE for $m \geq n_{match}$:

$$n_{m+1} = n_m + (1 + \lambda)^{m-n_{match}} \quad (33)$$

where λ was determined from the number of the desired mesh points. All calculations reported in this work were performed with the maximum cluster size equal to 50 000, the matching point of 10, and the total number of mesh points, including discrete rate equations, equal to 500. Increasing these values did not significantly change the resulting size distribution. Integration in time was performed using a variable-coefficient ordinary differential equation solver, VODE,[29] available through the ODEPACK Fortran library. In all cases, initial values of the scaled precursor concentration and the scaled cluster concentrations were set to unity and zero, respectively.

Results

The basic model described by eqs 13−15 is too complex to be solved analytically. A numerical solution, on the other hand, can be easily obtained with a reduced requirement for computational time by combining discrete rate equations for small clusters and discretized FPE (eq 31) for large clusters. The evolution of the size distribution, as represented by the scaled concentration, c_n, for a typical set of two main parameters, $\alpha = 10^8$ and $\beta = 10^1$, is presented in Figure 1a. The color of the 2-D plot corresponds to the log of the scaled concentration. The vertical cross sections allow us to visualize the change in the concentration of a given size cluster as a function of time, while the horizontal cross sections show the size distribution of clusters at any given time point. Several snapshots of the concentration profile at different values of τ are shown in Figure 1 b.

There are several experimentally relevant quantities that can be computed based on the concentration profile including the mean number (μ_n) and radius (μ_R), number (σ_n^2) and radial (σ_R^2) variance, reaction yield (Y), and total concentration of clusters (c_{tot}):

(25) Kashchiev, D. *Nucleation: Basic Theory with Applications*; Butterworth-Heinemann: Boston, MA, 2000.
(26) Chang, J. S.; Cooper, G. *J. Comput. Phys.* **1970**, *6* (1), 1–16.
(27) Epperlein, E. M. *J. Comput. Phys.* **1994**, *112* (2), 291–297.
(28) Sinno, T.; Brown, R. A. *J. Electrochem. Soc.* **1999**, *146* (6), 2300–2312.
(29) Brown, P. N.; Byrne, G. D.; Hindmarsh, A. C. *SIAM J. Sci. Stat. Comput.* **1989**, *10*, 1038–1051.

$$\mu_n = \langle n \rangle = \frac{\int n c_n \mathrm{d}n}{\int c_n \mathrm{d}n} \tag{34}$$

$$\mu_R = \langle R \rangle = \left(\frac{3}{4\pi\rho}\right)^{1/3} \langle n^{1/3} \rangle = \left(\frac{3}{4\pi\rho}\right)^{1/3} \frac{\int n^{1/3} c_n \mathrm{d}n}{\int c_n \mathrm{d}n} \tag{35}$$

$$\sigma_n^2 = \frac{\int (n - \langle n \rangle)^2 c_n \mathrm{d}n}{\int c_n \mathrm{d}n} \tag{36}$$

$$\sigma_R^2 = \left(\frac{3}{4\pi\rho}\right)^{2/3} \frac{\int (n^{1/3} - \langle n^{1/3} \rangle)^2 c_n \mathrm{d}n}{\int c_n \mathrm{d}n} \tag{37}$$

$$Y = 1 - p \tag{38}$$

$$c_{tot} = \int c_n \mathrm{d}n \tag{39}$$

In this work, we use CdSe number density, $\rho_{CdSe} = 17.8\ \mathrm{nm}^{-3}$, as the reference in calculation of the mean radius. For any other material, the mean radius can be obtained by:

$$\langle R \rangle = \langle R \rangle_{CdSe} \left(\frac{\rho_{CdSe}}{\rho}\right)^{1/3} \tag{40}$$

Note that the percent deviation in radius $((\sigma_R)/(\mu_R))$ is material independent.

Temporal evolution of the mean number size and one standard deviation above and below the mean are shown in Figure 1a. Evolution of the mean radius and the percent radial distribution are shown in Figure 1c. Evolution of the monomer and the total cluster concentration along with reaction yield are shown in Figure 1d. Examination of Figure 1c and d shows that there are five distinct regions in the behavior of the model that are summarized in Table 3. In region I, the precursor concentration remains effectively unchanged, while the monomer concentration increases approximately linearly with time until it reaches a maximum, when the rate of monomer depletion due to cluster growth, $(-(dc_1)/(d\tau))_g$, exceeds the rate of monomer formation from precursors. In region II, the precursor concentration still remains effectively unchanged, while the monomer is depleted and the mean cluster size and the percent size distribution are increased. The boundary between region II and III is defined by the maximum in the percent size distribution. As precursor concentration drops and the rate of monomer depletion due to growth decreases and the rate of monomer generation due to dissociation increases in region III, the mean size increases while the percent size distribution narrows. The focusing stops when the precursor is depleted leading to a pseudo steady state behavior in region IV, characterized by almost invariant monomer concentration, mean size, and size distribution. Note that in region IV, the total rate of monomer depletion and generation are equal but nonzero. Finally, in region V, the total rates of monomer depletion and generation decrease to zero, the mean size begins to increase and the percent size distribution broadens as the system slowly approaches the equilibrium distribution:

$$c_n = \frac{\beta}{\alpha}\left(\frac{\alpha}{\beta} c_1\right)^n n^{-2/3} \tag{41}$$

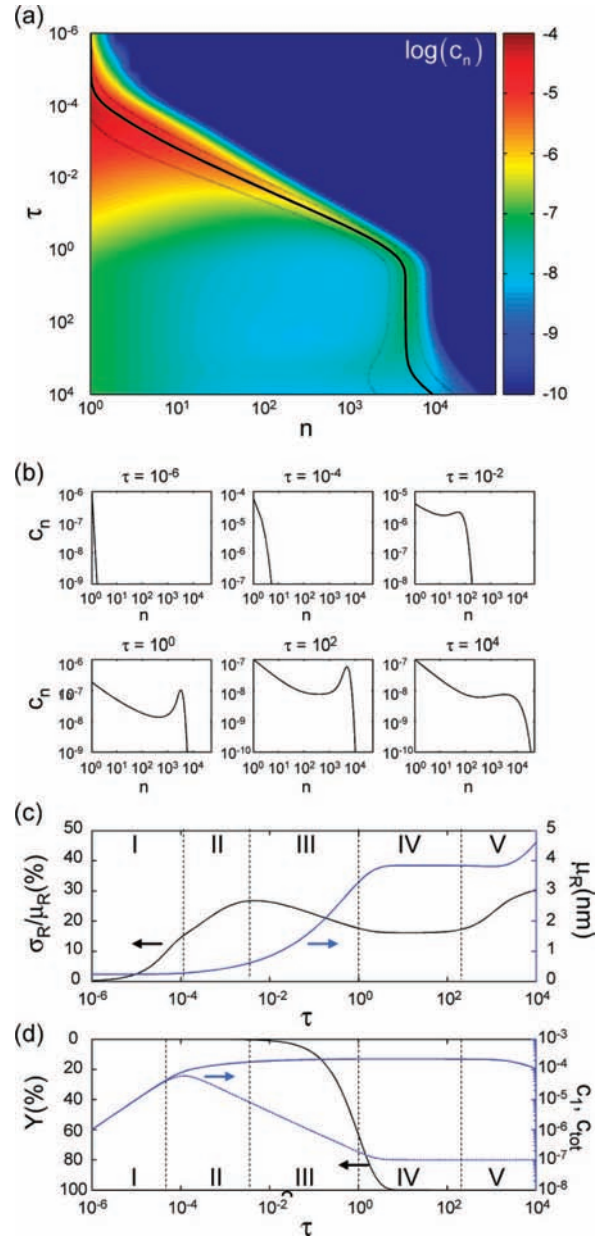

Figure 1. Model predictions for a typical set of parameters with $\alpha = 10^8$ and $\beta = 10^1$. (a) Concentration profile as a function of cluster size and scaled time. Color scale corresponds to the log of the concentration. The solid and dashed black lines correspond to the mean of the size distribution and one standard deviation above and below the mean. (b) Snapshots of the size distribution, c_n versus n, at different values of the scaled time. (c) Evolution of the mean radius computed for CdSe and percent radial distribution as a function of scaled time. (d) Evolution of the total cluster and monomer concentration and reaction yield as a function of the scaled time.

with reduced monomer concentration obtained implicitly from mass conservation.

Figure 2 illustrates the dependence of the model behavior on the values of the two parameters: α and β. In particular, the evolution of the mean radius and percent radial size distribution, Figure 2a and b, are shown for order of magnitude variation in α from 10^5 to 10^9 at two values of parameter β: 10^{-1} and 10^1. By increasing the scaled growth parameter α, the time onset of the focusing regime is decreased, while the time onset of the defocusing region is delayed. Increase in the scaled dissociation rate parameter β on the other hand, does not affect the onset of

Table 3. Description of Different Regions of Model Behavior Labeled in Figure 1c and d

Region	Observables	Rates
I-Generation of monomers	$c_1 \propto \tau$	$(p \sim 1) > \left(-\frac{dc_1}{d\tau}\right)_g > \left(\frac{dc_1}{d\tau}\right)_d \sim 0$
II-Small cluster formation, broadening	$c_1 \downarrow \mu_R \uparrow \frac{\sigma_R}{\mu_R} \uparrow$	$(p \sim 1) < \left(-\frac{dc_1}{d\tau}\right)_g$; $\left(\frac{dc_1}{d\tau}\right)_d \sim 0$
III-Focusing due to precursor depletion	$c_1 \downarrow \mu_R \uparrow \frac{\sigma_R}{\mu_R} \downarrow$	$(p \to 0) < \left(-\frac{dc_1}{d\tau}\right)_g \downarrow$; $\left(\frac{dc_1}{d\tau}\right)_d \uparrow$
IV-Invariant size and size distribution	$c_1\ \mu_R\ \frac{\sigma_R}{\mu_R}$ pss	$p \sim 0$; $0 < \left(-\frac{dc_1}{d\tau}\right)_g \approx \left(\frac{dc_1}{d\tau}\right)_d$
V-Increase in size and size distribution	$\frac{\sigma_R}{\mu_R} \uparrow \mu_r \uparrow$	$\left(-\frac{dc_1}{d\tau}\right)_g \downarrow \approx \left(\frac{dc_1}{d\tau}\right)_d \downarrow$

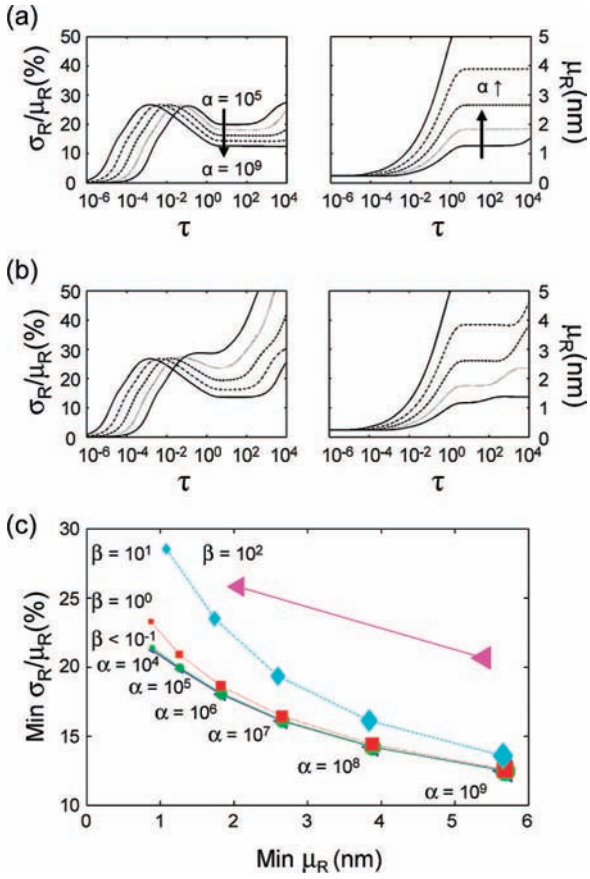

Figure 2. Evolution of the mean cluster radius computed for CdSe and the percent radial distribution at order of magnitude increments of scaled growth rate parameter α, ranging from 10^5 to 10^9 for (a) $\beta = 10^{-1}$ and (b) $\beta = 10^1$. (c) Minimum attained percent in the radial size distribution and the corresponding mean radial size at different values of the scaled growth and dissociation rate parameters α and β, respectively.

the focusing regime, but does accelerate the time onset of defocusing. Furthermore, for large values of β and small values of α the pseudo steady state regime is never reached, as demonstrated in Figure 2b in the case of $\alpha = 10^5$ and $\beta = 10^1$. For a set of parameters where the pseudo steady state regime is achieved, we can map out the minimum attained radial size distribution, Min $(\sigma_R)/(\mu_R)$, and the corresponding mean radius, Min μ_R, as shown in Figure 2c. In general, an increase in the scaled growth rate parameter α leads to larger mean radius and a smaller percent size distribution in the pseudo steady state regime. Furthermore, at a given value of α, an increase in β leads to a decrease in the mean size and an increase in the size distribution.

Temperature Modulation. Temperature plays an important role in the kinetics of nanocrystal formation, for example, synthetic routes incorporating an injection into a hot solvent have become widely accepted since the first demonstration.[8] To model this behavior, we modify the model to include temperature-induced variation in the rate of precursor conversion to monomer. We assume that the temperature is exponentially decaying from an initial value of T_0 to a final value of T_∞. Furthermore, we assume that the temperature effect on the cluster growth and dissociation rates is small relative to the effect on the monomer formation rate from precursors. Based on this assumption, the modified rate for precursor conversion to monomers is presented in eq 25 that incorporates three new parameters: scaled activation energy, ratio of final to initial temperatures, and the decay time of high temperature.

The evolution of the concentration profile with time for the same set of two main parameters as in Figure 1, $\alpha = 10^8$ and $\beta = 10^1$, with $\varepsilon_\infty = 30$, $\tau_T = 10^{-4}$, and $(T_\infty)/(T_0) = 0.8$ is shown in Figure 3a. The evolution of the mean radius and percent radial size distribution are shown in Figure 3c and d. The evolution of the monomer and total cluster concentrations with and without temperature modulation are shown in Figure 3e−f. Comparison of Figure 1a and Figure 3a and the curves in Figure 3c−f reveals that temperature modulation leads to a faster increase in the monomer concentration with the maximum monomer concentration being an order of magnitude larger with only a small decrease in the precursor concentration. Furthermore, once the temperature starts to decay, the monomer concentration stabilizes, leading to an emergence of a new regime with almost invariant cluster concentrations. Further generation of monomers at the reduced final temperature leads to focusing of the size distribution and an increase in the mean size. Once the precursor is depleted, the system approaches the pseudo steady state regime with a mean cluster size and percent size distribution both smaller than in the system with no temperature modulation. With the faster onset of the defocusing regime with temperature modulation, the system approaches the same equilibrium state as without temperature modulation, eq 41.

Figure 4a and b demonstrates how, for a given reduced activation energy, the choice of the magnitude and duration of the temperature increase affects the observed minimum radial

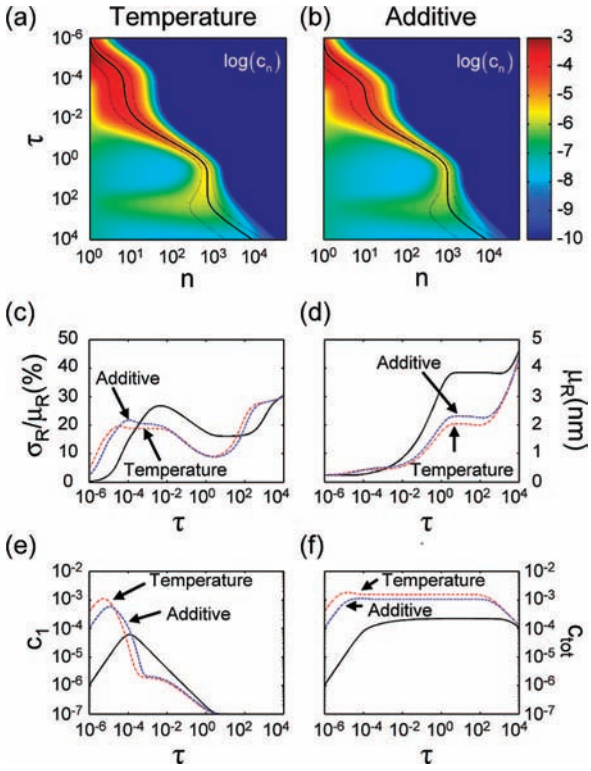

Figure 3. Comparison of model predictions in the absence and presence of temperature modulation ($\varepsilon_\infty = 30$, $\tau_T = 10^{-4}$, $(T_\infty)/(T_0) = 0.8$) or additives ($\delta = 10^2$, $a = 10^{-2}$) for the same set of the main model parameters shown in Figure 1, $\alpha = 10^8$ and $\beta = 10^1$. Concentration profile as a function of cluster size and scaled time in the case of (a) temperature modulation and (b) additives. Evolution of the (c) percent radial size distribution, (d) mean radius computed for CdSe, (e) monomer concentration, and (f) total cluster concentration as a function of scaled time in the case of temperature modulation (red), additives (blue), and the base model (black).

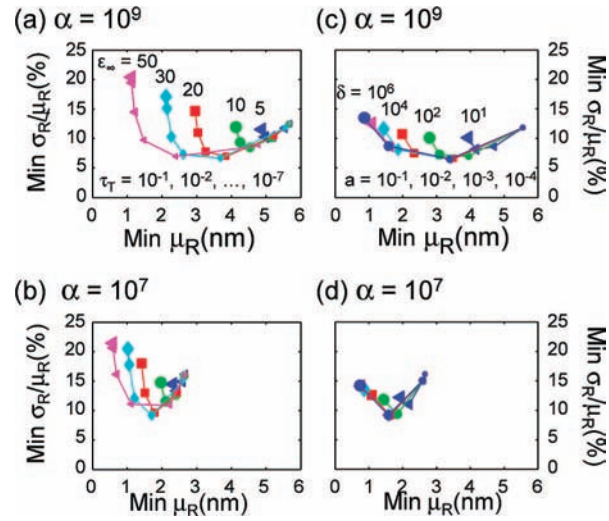

Figure 4. (a, b) Effect of temperature modulation on the minimum attained radial size distribution and the corresponding mean radius (CdSe) at different values of the scaled activation energy parameter, ε_∞, and the mean scaled temperature decay time, τ_T at $(T_\infty)/(T_0) = 0.8$. (c, d) Effect of additives at different values of the additive rate enhancement parameter δ and scaled additive content, a. In both cases, values are shown for $\beta = 10^{-3}$ and: (a, c) $\alpha = 10^7$ and (b, d) $\alpha = 10^9$. Increase in the marker size corresponds to an order of magnitude increase in the values of τ_T and a.

size distribution and the mean size. Values are shown at two different growth rates of α equal to 10^7 and 10^9. The data show that for short temperature pulses, the observed mean radial size and size distribution remain approximately unchanged. As shown in Figure 4a and b, intermediate values of the time duration lead to smaller sizes and size distributions. However, if the temperature remains high for too long, the precursor is depleted much faster and the duration of the focusing regime is greatly diminished, thus leading to a greater total number of clusters of smaller size with a broader size distribution. In general, higher growth rate, α, activation energy, ϵ_∞ (Figure 4), and initial to final temperature ratio, $(T_\infty)/(T_0)$ (data not shown), all lead to a more pronounced decrease in the size and the size distribution at lower values of τ_T. Thus, to minimize polydispersity, duration of the high temperature region must be reduced for higher values of these parameters.

Additives. Another factor that plays an important role in controlling nanocrystal formation is addition of species that can either accelerate or hinder the rate of precursor consumption. For example, impurities in tri-*n*-octylphosphine (TOP) in the synthesis of CdSe have a strong effect on controlling reaction kinetics. As discussed previously, certain additives can lead to much faster rates of precursor conversion to monomeric species. Assuming the concentration of additives is much smaller than that of precursors, and that the rate of conversion is much faster in the presence of additives, a modified rate of precursor conversion to monomers was introduced in eq 28. The modified expression contains two new parameters: relative additive content, a, and scaled rate enhancement factor, δ (Table 2). The evolution of the concentration profile with time at $\alpha = 10^8$ and $\beta = 10^1$, with $a = 1\%$ and $\delta = 10^2$ is shown in Figure 3b. The evolution of the mean radius, percent radial distribution, monomer concentration, and the total cluster concentration are shown in Figure 3c−f. Comparison of the concentration profiles between Figure 1a, Figure 3a, and Figure 3b shows that the effect of additives is similar to that of temperature decay, such that both lead to a pseudo steady state with the mean cluster size and percent size distribution at a lower value than in the system with no temperature modulation and no additives.

For a given intrinsic growth rate, α, the relative concentration and the enhancement in rate due to additives have a strong impact on the mean radial size and size distribution that can be achieved, Figure 4c and d. The data show that low concentrations of additives do not significantly change the observed mean radial size and size distribution. However, slightly higher concentrations of additives lead to smaller sizes and size distributions. Similar to the effect of long high temperature duration, high concentrations of additives can lead to significant depletion of precursors, thus reducing the duration of the focusing regime, leading to a greater total number of clusters of smaller size with broader distribution. Comparison of Figure 4c and d shows that at higher scaled growth rate, smaller amount of additives can achieve a significant decrease in both the mean size and size distribution. Furthermore, increasing the strength of the additive enhances the focusing for intermediate concentrations of additives; however, at higher additive content it can also lead to smaller sizes and broader distributions.

Discussion

In this work, we have developed a kinetic model of nucleation and growth that can be applied to describe the liquid phase synthesis of nanocrystals. The model assumes that following a slow process of precursor conversion to monomers, monomers combine to form dimers, then trimers, then larger and larger clusters. Nondimensionalization of the model allows us to reduce

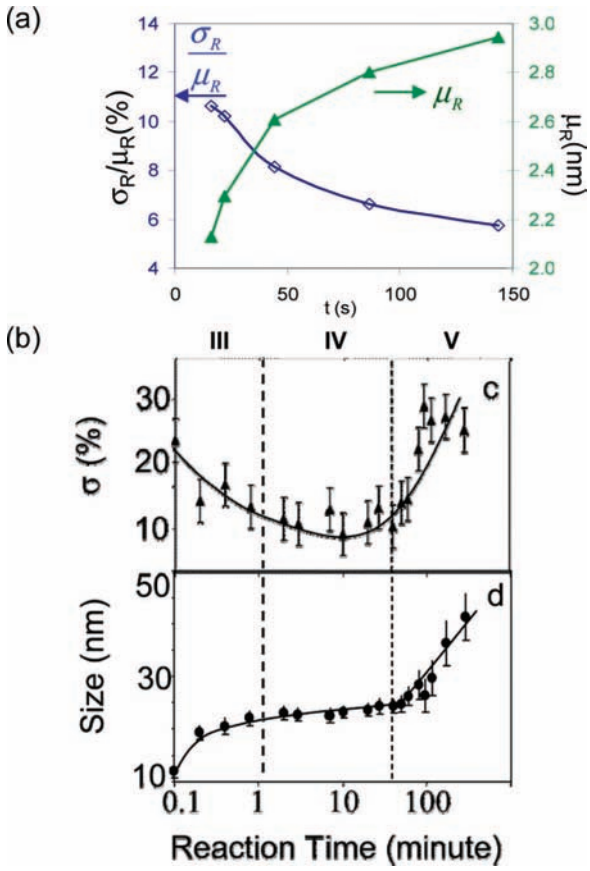

Figure 5. (a) Mean radius and percent in the radial size distribution as a function of residence time in the synthesis of CdSe nanocrystals using a capillary reactor. (b) Time evolution of the percent in the radial size distribution and mean radius in the synthesis of MnO particles. Figure reproduced from Chen, et al. *J. Am. Chem. Soc.* **2007**, *129* (35). Figure reproduced from Yen et al. *Advanced Materials* **2003**, *15* (21).

the number of variables and constants to two nondimensional parameters, α and β, that correspond to scaled growth and dissociation rates, respectively. Thus, a single set of values of α and β can be used to describe a variety of experimental conditions. Furthermore, combining discrete rate equations for small sized clusters and discretization of the corresponding continuous Fokker−Planck equation for larger sized clusters significantly reduces the computational intensity of the problem, while at the same time retaining a maximum amount of information. For example, interpolation of the results allows us to track the concentration of every sized cluster as a function of time. Consequently, it not only gives information about the evolution of the mean and the variance, but also the exact shape of the size distribution.

It is important to compare the phenomenological behavior of the model with experimental observations at different time scales. Data from Yen et al.[30] reproduced in Figure 5a shows the evolution of the CdSe nanocrystal mean radius and percent in the radial size distribution as a function of the residence time. However, a problem arises at short times, where growth solution post processing makes it difficult to extract information on the entire size distribution for small clusters. For larger nanocrystals this information is much more readily available, as demonstrated in the case of MnO synthesis[31] (Figure 5b). First, at short times, the model corroborates the experimental observation of an increase in the mean nanocrystal size and a simultaneous focusing of the percent size distribution. The observed radial size distributions are shown to be on the order of 10−20%, which are similar to the results obtained experimentally at the most favorable experimental conditions. Second, the model predicts that the focusing region is followed by a pseudo steady state region with an almost invariant mean size and size distribution. Again, this has also been observed experimentally both for MnO and CdSe, as evident by region IV of Figure 5a and an asymptotic approach to steady state in Figure 5b, respectively. Finally, at long times the distribution shifts to larger sizes with a simultaneous increase in the percent size distribution and a decrease in the total number of nuclei, region V of Figure 5b. This explains why, to achieve a narrow size distribution, the synthesis of nanocrystals is thermally quenched once the desired size is attained. Thus, in the time scales that can be resolved experimentally, regions III, IV, and V of the model that correspond to the focusing, pseudo steady state, and defocusing regimes, match the experimental observations.

Another important aspect of the model is its simplicity. The model has only two main parameters, $\alpha = (k_a P_0)/(k_f)$ and $\beta = (k_d)/(k_f)$, that can be used as experimental guides in tuning the operating conditions to achieve the desired nanocrystal size and size distribution. For example, by increasing α, we can increase the mean size and decrease the minimum in the size distribution achieved during focusing. Also, by decreasing β or by increasing α, we can extend the onset of defocusing, thus allowing for a broader time window to achieve maximum narrowing of the size distribution. There are several ways these parameters can be adjusted experimentally. First, the initial concentration of precursors can be increased to increase α. Second, the rate of monomer addition, k_a:

$$k_a \propto \frac{1}{1 + K_{eq}L} \tag{42}$$

can be increased by decreasing the ligand concentration or introducing weaker binding ligands. Steric effects would also suggest that smaller monomers would exhibit a higher rate of addition; therefore, since monomers are stabilized by ligands, shortening the hydrocarbon chain lengths on the ligands would lead to an increase in k_a. Third, the rate of dissociation, k_d:

$$k_d \propto \frac{K_{eq}L}{1 + K_{eq}L} \tag{43}$$

prior to cluster surface saturation, $K_{eq}L < 1$, can be decreased by decreasing ligand concentration or by utilizing weaker binding ligands. Furthermore, introducing ligands that bind weaker to the monomers is another way of decreasing the dissociation rate. Lastly, the rate of precursor conversion to monomers, k_f, can be increased by substituting more reactive precursors. Note that the model does not include cluster aggregation, which might become a problem if ligands are too loosely bound and do not effectively stabilize the nanocrystals.

Another important way the reaction can be controlled is by changing the temperature, and thus changing the rate of precursor conversion to monomers. Performing the reaction at a lower temperature, thus decreasing k_f, leads to an increases

(30) Yen, B. K. H.; Stott, N. E.; Jensen, K. F.; Bawendi, M. G. *Adv. Mater.* **2003**, *15* (21), 1858–1862.

(31) Chen, Y.; Johnson, E.; Peng, X. *J. Am. Chem. Soc.* **2007**, *129* (35), 10937–10947.

in α and β parameters and an increase in the real time that corresponds to a given value of τ. The faster scaled addition rate would allow for larger nanocrystals with narrower size distributions. However, if the temperature is too low, where dissociation becomes important, a higher value of β would also lead to faster onset of defocusing thus, decreasing the time window for focusing. As a result, temperature must be chosen carefully to balance the growth and dissociation contributions. As the guiding principle for experiments, the simplest way to estimate the value of k_f is by observing the time required to reach a reaction yield of 50%:

$$k_{\mathrm{f}} = \frac{-\ln(2)}{t_{1/2}} \tag{44}$$

The Arrhenius form of k_{f} can be obtained from experimental values of $t_{1/2}$ at different temperatures. For example, for the synthesis of CdSe in the method described by Yen et al.,[30] the activation energy for the precursor conversion reaction is approximately 20 kcal/mol with pre-exponential factor of $4 \cdot 10^5$ s^{-1}. In the temperature range considered, 220−320 °C, there is at most an order of magnitude variation in k_{f} with the yield approaching 70% at higher temperatures.

Much importance in the experimental literature is placed on the necessity of the diffusion limitation to observe size distribution focusing based on simple first order reaction and diffusion model for a single particle growth.[14,15] To test this hypothesis, we can estimate the rate of growth under diffusion limitation and compare it to the experimental observations. Under diffusion limitation, the flux of monomers to the cluster must equal the rate of cluster growth:

$$\frac{4\pi R^2}{V_m}\frac{\mathrm{d}R}{\mathrm{d}t} = 4\pi D R C_m \tag{45}$$

where V_m is the molar volume, D is the diffusivity, and C_m is the concentration of the monomers. Using Stokes−Einstein relation, a typical value for monomer diffusivity would be on the order of $10^{-11} - 10^{-9}$(m^2)/(s). Therefore, for nanocrystals with a final radius on the order of a few nanometers, the estimated diffusion limited radial growth rate would be:

$$\frac{\mathrm{d}R}{\mathrm{d}t} = \frac{D}{R}V_m C_m \approx \frac{10^{-11}\frac{\mathrm{m}^2}{\mathrm{s}}}{10^{-9}m} \times 10^{-28}m^3 \times 10^{25}m^{-3} = 10^{-5}\frac{\mathrm{m}}{\mathrm{s}} \tag{46}$$

Under typical experimental conditions however, the nanocrystals grow at most 1 (nm)/(s), which is several orders of magnitude slower than the diffusion limited estimate.

To further explore this issue, we compare the behavior of the model under reaction and diffusion limitation (eq 23). In general, the diffusion limited growth model behaves similarly to the reaction limited growth exhibiting the precursor conversion to monomers, decay in monomer concentration, focusing, pseudo steady state, and defocusing regimes. Figure 6 shows the minimum attained radial size distribution and the corresponding mean radius as a function of the scaled growth parameters α and α_D for reaction and diffusion controlled conditions, respectively. The data show that for small mean cluster sizes, diffusion limitation does lead to narrower size distributions, with an improvement of about 5% in the radial distribution. However, for larger clusters, $n > 4000$, $R_{\mathrm{CdSe}} > 4$ nm, in the size region where diffusion limitation is likely to be

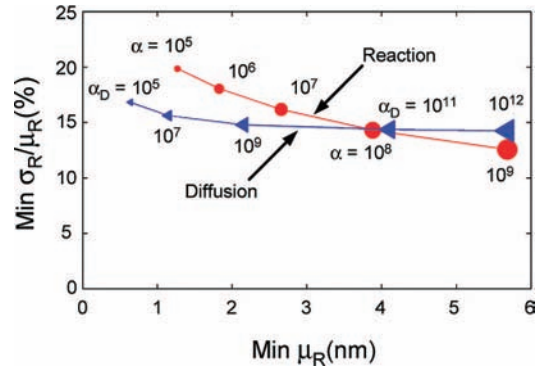

Figure 6. Minimum attained radial size distribution and the corresponding mean radius computed for CdSe at different values of the growth rate parameter α under reaction ($g_n \propto n^{2/3}$) and α_D under diffusion ($g_n \propto n^{1/3}$) limitation.

of primary concern, reaction control leads to narrower distributions. Furthermore, our model indicates that focusing of the size distribution can be achieved under pure reaction control, where the growth rate is proportional to the surface area ($\sim n^{2/3}$). To our knowledge, this is the first time that this has been demonstrated.

As shown in Figure 2, the model predicts that larger nanocrystals with narrower size distributions can be prepared by increasing the growth rate parameter, α. At the same time, it is not obvious how to prepare small nanocrystals with narrow size distributions. This has also been the case experimentally: the smaller the desired final size of the nanocrystal, the more difficult it is to find the optimal conditions for their synthesis. In Figure 4 we show that generation of small and narrowly distributed nanocrystals can be achieved using either temperature modulation or targeted introduction of additives. In the first approach, the idea is to start the reaction at high temperature, inducing fast generation of small clusters and depletion of monomers, and then to let the temperature decay to allow for slow growth as more monomers are produced from precursors. For a given chemistry, duration of high temperature, growth rate, and ratio of initial to final temperature can be optimized to achieve a desired size and minimize the size distribution. This is similar to the idea of the hot solvent injection method used for the batch synthesis of nanocrystals.[8] The second approach is to introduce small quantities of additives that lead to faster rates of precursor conversion, making more monomers and inducing fast formation of small clusters. As the additive is depleted, the reaction slows down, leading to larger total concentration of smaller sized nanocrystals with narrower distributions. Again, the additive content and strength can be systematically varied to produce the desired size and minimize the size distribution. In practice, the additive effect would also explain why, for the same synthetic route yielding CdSe under the same conditions, different batches of tri-*n*-octylphosphine can produce nanocrystal samples with drastically different sizes and size distributions.

Conclusions

In summary, we have developed a kinetic model to describe the combined phenomena nanocrystal nucleation and growth. The model is general and can be applied to describe the synthesis of many different types of nanocrystals under a variety of experimental conditions. Furthermore, the simplicity of the nondimensional model with only two parameters yields a better

understanding of the nanocrystal formation process and allows for a rational modification of the experimental conditions to achieve desired sizes and size distributions of nanocrystals. The model also shows that, contrary to the accepted hypothesis, diffusion limitation is not required for size distribution focusing, and that focusing is achieved under pure reaction control. In addition, the model allows us to test different schemes for generation of small nanocrystals with narrow size distributions, for example, by either modulating temperature or by targeted introduction of additives. In the future, using the formalism developed in this work, it would be possible to develop a more refined understanding of the nanocrystal formation process. For example, coupling the model with a detailed description of the precursor activation chemistry, based on experiments or first-principles calculations, can yield a better understanding of what role specific precursors, ligands, and additives play in the nanocrystal formation process.

Acknowledgment. Financial support was provided in part by the U.S. Army through the Institute for Soldier Nanotechnologies, under Contract DAAD-19-02-0002 with the U.S. Army Research Office and by the Hertz Foundation graduate fellowship to J.R.

Supporting Information Available: Discretization of the Fokker-Plank Equation (FPE) and boundary conditions. This material is available free of charge via the Internet at http://pubs.acs.org.

JA809156T